

Leading Loop Effects in Pseudoscalar-Higgs Portal Dark Matter

Karim Ghorbani*

*Physics Department, Faculty of Sciences, Arak University,
Arak 38156-8-8349, Iran*

Parsa Hossein Ghorbani†

*APPLIED PHYSICS, Center for Research in Astrophysics and Cosmology,
300 Park Avenue, New York, NY 10022, USA*

Abstract

We examine a model with a fermionic dark matter candidate having pseudoscalar interaction with the standard model particles where its direct detection elastic scattering cross section at tree level is highly suppressed. We then calculate analytically the leading loop contribution to the spin independent scattering cross section. It turns out that these loop effects are sizable over a large region of the parameter space. Taking constraints from direct detection experiments, the invisible Higgs decay measurements, observed DM relic density, we find viable regions which are within reach in the future direct detection experiments such as XENONnT.

1 Introduction

A nagging question in contemporary modern physics is about the nature of dark matter (DM) and its feasible non-gravitational interaction with the standard model (SM) particles. This problem is in fact deemed straddling both particle physics and cosmology.

On the cosmology side, precise measurements of the Cosmic Microwave Background (CMB) anisotropy not only demonstrate the existence of dark matter but also provide us with the current dark matter abundance in the universe [1, 2]. On the particle physics side, the dedicated search is to find direct detection (DD) of the DM interaction with the ordinary matter via Spin Independent (SI) or Spin Dependent (SD) scattering of DM-nucleon in underground experiments like LUX [3], XENON1T [4] and PandaX-II [5]. Although in these experiments the enticing signal is not shown up so far, the upper limit on the DM-matter interaction strength is provided for a wide range of the DM mass. Among various candidates for particle DM, the most sought one is the Weakly Interacting Massive Particle (WIMP).

*karim1.ghorbani@gmail.com

†parsa@appliedphysics.org

Within WIMP paradigm there exist a class of models where SI scattering cross section is suppressed significantly at leading order in perturbation theory, hence the model eludes the experimental upper limits in a large region of the parameter space. The interaction type of the WIMP-nucleon in these models are pseudoscalar or axial vector at tree level resulting in momentum or velocity suppressed cross section [6]. The focus here is on models with pseudoscalar interaction between the DM particles and the SM quarks. In this case there are both SI and SD elastic scattering of the DM off the nucleon at tree level. Both type of the interactions are momentum dependent while the SD cross section gets suppressed much stronger than the SI cross section due to an extra momentum transfer factor, q^2 . Thus, in these models taking into account beyond tree level contributions which could be leading loop effects or full one-loop effects are essential.

We recall several earlier works done in this direction with emphasis on DM models with a pseudoscalar interaction. Leading loop effect on DD cross section is studied in an extended two Higgs doublet model in [7, 8, 9]. Within various DM simplified models in [10, 11, 12] and in a singlet-doublet dark matter model in [13] the loop induced DD cross sections are investigated. Full one-loop contribution to the DM-nucleon scattering cross section in a Higgs-portal complex scalar DM model can be found in [14]. In [15] direct detection of a pseudo scalar dark matter is studied by taking into account higher order corrections both in QCD and non-QCD parts.

In this work we consider a model with fermionic DM candidate, ψ , which interacts with a pseudoscalar mediator P as $P\bar{\psi}\gamma^5\psi$. The pseudoscalar mediator will be connected to the SM particles via mixing with the SM Higgs with an interaction term as $PH^\dagger H$. In this model the DM-nucleon interaction at tree level is of pseudoscalar type and thus its scattering cross section is highly suppressed over the entire parameter space. The leading loop contribution to the DD scattering cross section being spin independent is computed and viable regions are found against the direct detection bounds. Beside constraints from observed relic density, the invisible Higgs decay limit is imposed when it is relevant.

The outline of this article is as follows. In Sec. 2 we recapitulate the pseudoscalar DM model. We then present our main results concerning the direct detection of the DM including analytical formula for the DD cross section and numerical analysis in Sec. 3. Finally we finish with a conclusion.

2 The Pseudoscalar Model

The model we consider in this research as a renormalizable extension to the SM, consists of a new gauge singlet Dirac fermion as the DM candidate and a new singlet scalar acting as a mediator, which connects the fermionic DM to SM particles via the Higgs portal. The new physics Lagrangian comes in two parts,

$$\mathcal{L} = \mathcal{L}_{\text{DM}} + \mathcal{L}_{\text{scalar}} . \quad (1)$$

The first part, \mathcal{L}_{DM} , introduces a pseudoscalar interaction term as

$$\mathcal{L}_{\text{DM}} = \bar{\psi}(i\partial\!\!\!/ - m_{\text{dm}})\psi - ig_d P\bar{\psi}\gamma^5\psi , \quad (2)$$

and the second part, $\mathcal{L}_{\text{scalar}}$, incorporates the singlet pseudoscalar and the SM Higgs doublet as

$$\begin{aligned}\mathcal{L}_{\text{scalar}} = & \frac{1}{2}(\partial_\mu P)^2 - \frac{m^2}{2}P^2 - \frac{g_3}{6}P^3 - \frac{g_4}{24}P^4 + \mu_H^2 H^\dagger H \\ & - \lambda(H^\dagger H)^2 + g_0 P - g_1 P H^\dagger H - g_2 P^2 H^\dagger H.\end{aligned}\quad (3)$$

The pseudoscalar field is assumed to acquire a zero vacuum expectation value (vev), $\langle P \rangle = 0$, while it is known that the SM Higgs develops a non-zero vev where $\langle H \rangle = v_h = 246$ GeV. Having chosen $\langle P \rangle = 0$, the tadpole coupling g_0 is fixed appropriately. After expanding the Higgs doublet in unitary gauge as $H = (0 \ v_h + h')^T$, we write down the scalar fields in the basis of mass eigenstates h and s , in the following expressions

$$h' = h \cos \theta - s \sin \theta, \quad P = h \sin \theta + s \cos \theta. \quad (4)$$

The mixing angle, θ , is induced by the interaction term $PH^\dagger H$ and is obtained by the relation $\sin 2\theta = 2g_1 v_h / (m_h^2 - m_s^2)$, in which $m_h = 125$ GeV and m_s are the physical masses for the Higgs and the singlet scalar, respectively. The quartic Higgs coupling is modified now and is given in terms of the mixing angle and the physical masses of the scalars as $\lambda = (m_h^2 \cos^2 \theta + m_s^2 \sin^2 \theta) / (2v_h^2)$. We can pick out as independent free parameters a set of parameters as $\theta, g_d, g_2, g_3, g_4$ and m_s . The coupling g_1 is then fixed by the relation $g_1 = \sin 2\theta (m_h^2 - m_s^2) / (2v_h)$. Recent study on the DM and the LHC phenomenology of this model can be found in [16, 17] and its electroweak baryogenesis is examined in [18].

For DM masses in the range $m_{\text{dm}} < m_h/2$, one can impose constraint on the parameters g_d, θ and m_{dm} from invisible Higgs decay measurements with $\text{Br}(h \rightarrow \text{invisible}) \lesssim 0.24$ [19]. Given the invisible Higgs decay process, $h \rightarrow \bar{\psi}\psi$, we find for small mixing angle the condition $g_d \sin \theta \lesssim 0.16 \text{ GeV}^{1/2} / (m_h^2 - 4m_{\text{dm}}^2)^{1/4}$ [20].

We compute DM relic density numerically over the model parameter space by applying the program `micrOMEGAs` [21]. The observed value for the DM relic density used in our numerical computations is $\Omega h^2 = 0.1198 \pm 0.0015$ [22]. The DM production in this model is via the popular freeze-out mechanism [23] in which it is assumed that DM particles have been in thermal equilibrium with the SM particles in the early universe.

We find the viable region in the parameter space respecting the constraints from observed relic density and invisible Higgs decay in Fig. 1. The parameters chosen in this computation are $\sin \theta = 0.02$, $g_3 = 200$ GeV and $g_2 = 0.1$. It is evident in the plot that regions with $m_{\text{dm}} < m_h/2$ are excluded by the invisible Higgs decay constraints. The analytical formulas for the DM annihilation cross sections are given in appendix A.

3 Direct Detection

In the model we study here the DM interaction with the SM particles is of pseudoscalar type, and at tree level its Spin Independent cross section is obtained in the following formula

$$\sigma_{\text{SI}}^p = \frac{2}{\pi} \frac{\mu^4 A^2}{m_{\text{dm}}^2} v_{\text{dm}}^2, \quad (5)$$

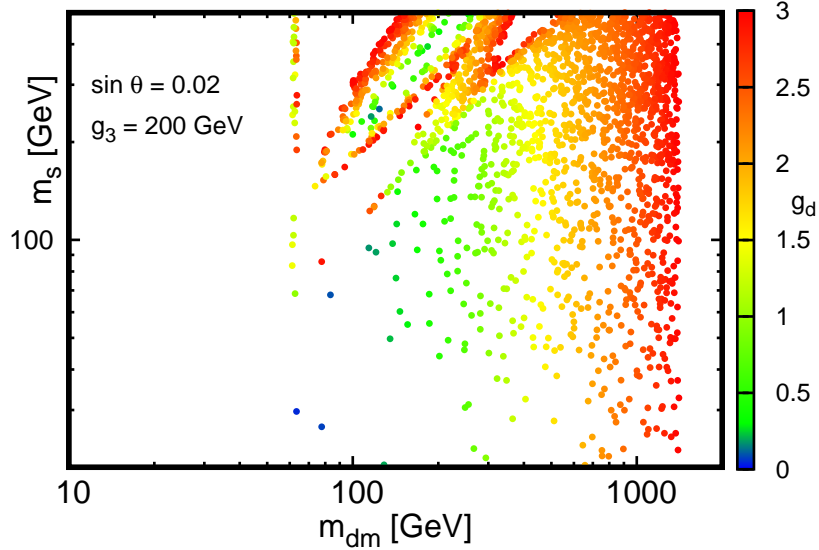


Figure 1: The viable region shown in the $m_s - m_{\text{dm}}$ plane respects the restrictions from observed relic density and measurements of the invisible Higgs decay.

where μ is the reduced mass of the DM and the proton, $v_{\text{dm}} \sim 10^{-3}$ is the DM velocity, and A is given by

$$A = \frac{g_d \sin 2\theta}{2v_h} \left(\frac{1}{m_h^2} - \frac{1}{m_s^2} \right) \times 0.28 m_p, \quad (6)$$

where the number 0.28 incorporates the hadronic form factor and m_p denotes the proton mass. Therefore, the DM-nucleon scattering cross section is velocity suppressed at tree level. Other words, the entire parameter space of this model resides well below the reach of the direct detection experiments. The current underground DD experiments like LUX [3] and XENON1T [4] granted us with the strongest exclusion limits for DM mass to be in the range ~ 10 GeV up to ~ 10 TeV. The future DD experiments can only probe direct interaction of the DM-nucleon down to the cross sections comparable with that of the neutrino background (NB), $\sigma_{\text{NB}} \sim \mathcal{O}(10^{-13})$ pb [24]. In the present model, as we will see in our numerical results the tree level DM-nucleon DD cross section is orders of magnitude smaller than NB cross sections. For such a model with the DM-nucleon cross section being velocity-suppressed at tree level, it is mandatory to go beyond tree level and find the SI cross section. The leading diagrams (triangle diagrams) contributing to the SI cross section are drawn in Fig. 2. There are also contributing box diagrams to the DM-nucleon scattering process. The box diagrams bring in a factor of m_q^3 (q stands for light quarks) as shown in [25], while the triangle diagrams are proportional to m_q . Thus, we consider the box diagrams to have sub-leading effects. We then move on to compute the leading loop effects on the SI scattering cross section. In the following we write out the full expression for the DM-quark scattering amplitude when scalars in the triangle loop have masses m_i and m_j and that coupled to quarks has mass m_k ,

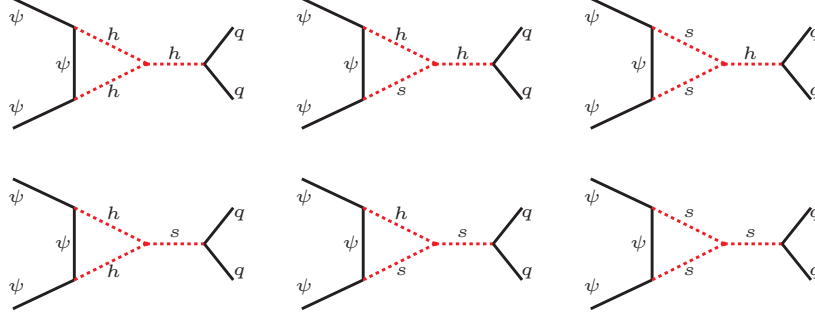


Figure 2: The leading loop diagrams for DM Spin Independent elastic scattering off the SM quarks.

$$i\mathcal{M}^{ijk} = \left[\frac{C_k}{(p_1 - p_2)^2 - m_k^2} \right] \bar{q}q \times \int \frac{d^4q}{(2\pi)^4} \frac{g_d^2 \bar{\psi}(p_2) \gamma^5 (\not{q} + m_{\text{dm}}) \gamma^5 \psi(p_1)}{[(p_2 - q)^2 - m_i^2][(p_1 - q)^2 - m_j^2][q^2 - m_{\text{dm}}^2]}. \quad (7)$$

In the above, the indices i, j and k stand for the Higgs (h) or the singlet scalar (s). In the expression above, we have $C_h = -m_q/v_h \cos \theta$ and $C_s = m_q/v_h \sin \theta$. The corresponding effective scattering amplitude in the limit that the momentum transferred to a nucleon is $q^2 \sim 0$, follows this formula,

$$i\mathcal{M}_{\text{eff}}^{ijk} = -i \frac{m_{\text{dm}} g_d^2}{16\pi^2} C_{ijk} F(\beta_i, \beta_j) \frac{C_k}{m_k^2} (\bar{q}q)(\bar{\psi}\psi), \quad (8)$$

in which $\beta_i = m_i^2/m_{\text{dm}}^2$ and $\beta_j = m_j^2/m_{\text{dm}}^2$, and the loop function $F(\beta_i, \beta_j)$ is given in appendix B. In the cases that the two scalar masses in the triangle loop are identical, i.e. $m_i = m_j$, then let's take $\beta_i = \beta_j$ and represent $F(\beta_i, \beta_j)$ by $F(\beta_i)$ which is provided by appendix B. The validity of these loop functions are verified upon performing numerical integration of the Feynman integrals and making comparison for a few distinct input parameters. C_{ijk} is the trilinear scalar coupling, where there are four of them corresponding to the vertices hhh , hhs , ssh and sss as appeared in Fig. 2.

Putting together all the six triangle diagrams, we end up having the expression below for the total effective SI scattering amplitude,

$$\begin{aligned} \mathcal{M}_{\text{eff}} &= \frac{m_q}{v_h} \frac{m_{\text{dm}} g_d^2}{16\pi^2} \left[\frac{\cos \theta}{m_h^2} C_{hhh} F(\beta_h) + \frac{\cos \theta}{m_h^2} C_{hsh} F(\beta_h, \beta_s) + \frac{\cos \theta}{m_h^2} C_{ssh} F(\beta_s) \right. \\ &\quad \left. - \frac{\sin \theta}{m_s^2} C_{hhs} F(\beta_h) - \frac{\sin \theta}{m_s^2} C_{hss} F(\beta_h, \beta_s) - \frac{\sin \theta}{m_s^2} C_{sss} F(\beta_s) \right] (\bar{q}q)(\bar{\psi}\psi) \\ &\equiv m_q \alpha (\bar{q}q)(\bar{\psi}\psi), \end{aligned} \quad (9)$$

The Spin Independent DM-proton scattering is

$$\sigma_{\text{SI}}^p = \frac{4\alpha_p^2 \mu^2}{\pi}, \quad (10)$$

in which μ is the reduced mass of the DM and the proton, and

$$\alpha_p = m_p \alpha \left(\sum_{q=u,d,s} F_{T_q}^p + \frac{2}{9} F_{T_g}^p \right) \sim 0.28 m_p \alpha, \quad (11)$$

where m_p is the proton mass and the quantities $F_{T_q}^p$ and $F_{T_g}^p$ define the scalar couplings for the strong interaction at low energy. The trilinear couplings in terms of the mixing angle and the relevant couplings in the Lagrangian and, the DD cross section at tree and loop level are given in appendix B. The scalar form factors used in our numerical computations are, $F_u^p = 0.0153$, $F_d^p = 0.0191$ and $F_s^p = 0.0447$ [26]. To obtain the scalar form factors, the central values of the following sigma-terms are used, $\sigma_{\pi N} = 34 \pm 2$ MeV and $\sigma_s = 42 \pm 5$ MeV. We computed the correction to the DD cross section at loop-level by including the uncertainty on the two sigma-terms. We found that the corresponding uncertainty on the DD cross section are not big enough to be seen in the plots. However, we estimated the uncertainty for a given benchmark point with $m_{\text{dm}} \sim 732$ GeV, $g_d \sim 2.17$, $g_3 = 10$ GeV and $\sin \theta = 0.02$. The result is $\sigma_{\text{loop}}^p = (3.084 \pm 0.12) \times 10^{-10}$ pb.

In the first part of our scan over the parameter space we wish to compare the DM-proton SI cross section at tree level with the SI cross section stemming from leading loop effects. To this aim, we consider for the DM mass to take values as $10 \text{ GeV} < m_{\text{dm}} < 2 \text{ TeV}$, and the scalar mass in the range $20 \text{ GeV} < m_s < 500 \text{ GeV}$. The dark coupling varies such that $0 < g_d < 3$. The mixing angle in these computations is chosen a small value being $\sin \theta = 0.02$. Reasonable values are chosen for the couplings, $g_2 = 0.1$ and $g_4 = 0.1$. Taking into account constraints from Planck/WMAP on the DM relic density, we show the viable parameter space in terms of the DM mass and g_d in Fig. 3 for two distinct values of the coupling g_3 fixed at 10 GeV and 200 GeV. Regions excluded by the invisible Higgs decay measurements are also shown in Fig. 3. As expected the tree level SI cross section is about 10 orders of magnitude below the neutrino background. On the other hand, for both values of g_3 , the leading loop effects are sizable in a large portion of the parameter space. A general feature apparent in the plots is that for $g_d \gtrsim 2.5$, the DM mass smaller than 600 GeV gets excluded by direct detection bounds.

In addition, with the same values in the input parameters, we show the viable regions in terms of the DM mass and the single scalar mass in Fig. 4. It is found that in both cases of the coupling g_3 , a wide range of the scalar mass, i.e, $10 \text{ GeV} < m_s < 500 \text{ GeV}$ lead to the SI cross sections above the neutrino floor. It is also evident from the results in Fig. 4 that the viable region with $m_s \sim 10 \text{ GeV}$ located at $m_{\text{dm}} \lesssim 100 \text{ GeV}$ in the case that $g_3 = 10 \text{ GeV}$, is shifted to regions with $m_{\text{dm}} \gtrsim 250 \text{ GeV}$ in the case that $g_3 = 200 \text{ GeV}$.

In the last part of our computations we perform an exploratory scan in order to find the region of interest which are the points with the SI cross sections above the neutrino floor and below the DD upper limits, with other constraints imposed including the observed DM relic density and the invisible Higgs decay. The scan is done with these input parameters: $10 \text{ GeV} < m_{\text{dm}} < 2 \text{ TeV}$, $20 \text{ GeV} < m_s < 1 \text{ TeV}$, $0 < g_d < 3$, $g_1 = g_4 = 0.1$ and g_3 fixed at 200 GeV. Our results are shown in Fig. 5. The mixing angle is set to $\sin \theta = 0.02$ in the left panel and $\sin \theta = 0.07$ in the right panel. It can be seen that for larger mixing angle the viable region is slightly broadened towards heavy pseudoscalar masses for the DM mass $60 \text{ GeV} < m_{\text{dm}} < 300 \text{ GeV}$, also is shrank towards regions with $m_{\text{dm}} \gtrsim 60 \text{ GeV}$ due to the invisible Higgs decay constraint. We also realize that if we confine ourselves to dark coupling

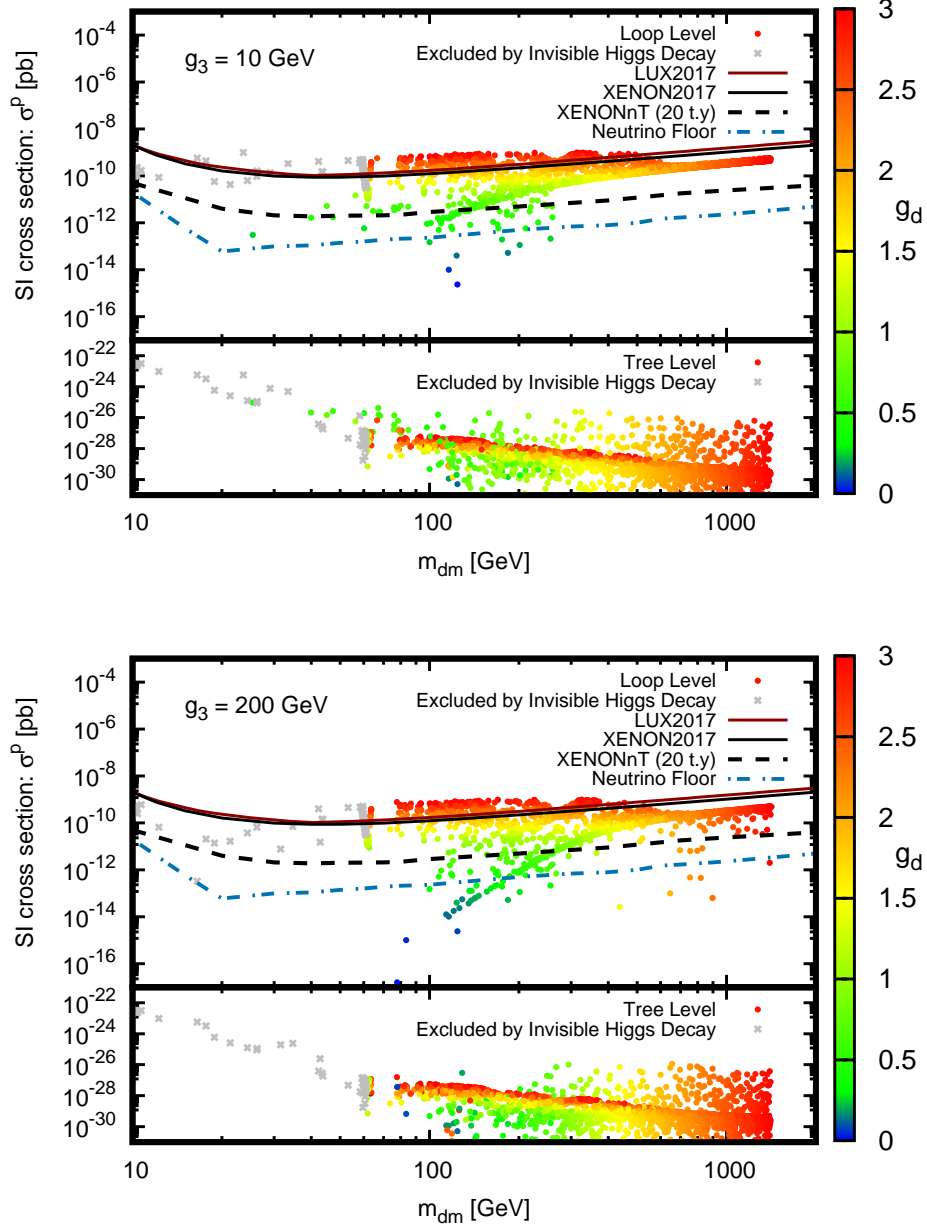


Figure 3: Shown are the DM-proton scattering cross section against the DM mass. In the upper panel $g_3 = 10$ GeV and in the lower panel $g_3 = 200$ GeV. The mixing angle is such that $\sin \theta = 0.02$. The vertical color spectrum indicates the range of the dark coupling g_d . Here, the observed relic density constraint is applied, The upper limits from LUX and XENON1T and also XENONnT projection are shown.

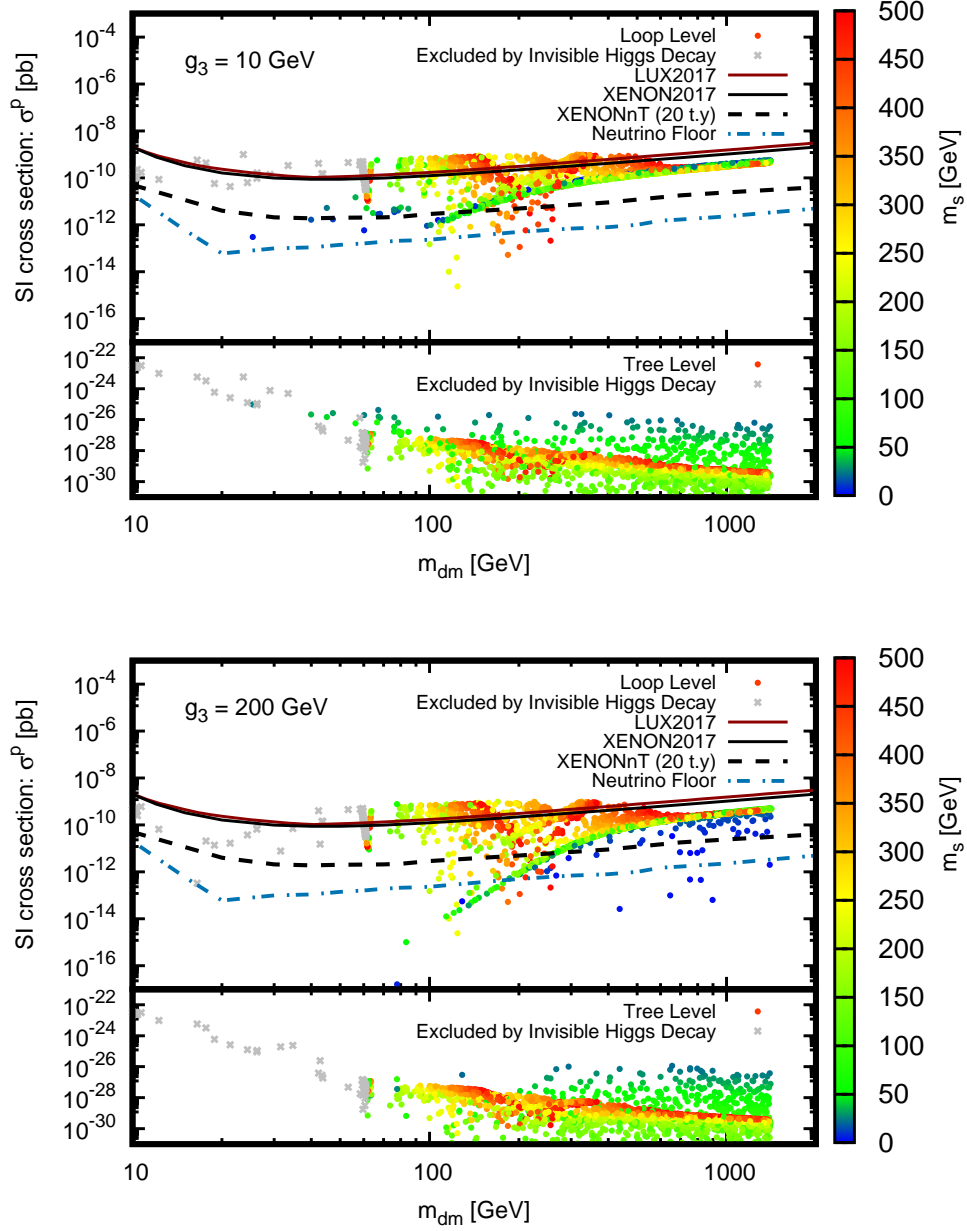


Figure 4: Shown are the DM-proton scattering cross section against the DM mass. In the upper panel $g_3 = 10$ GeV and in the lower panel $g_3 = 200$ GeV. The mixing angle is such that $\sin \theta = 0.02$. The vertical color spectrum indicates the range of the singlet scalar mass, m_s . Here, the observed relic density constraint is applied, The upper limits from LUX and XENON1T and also XENONnT projection are shown.

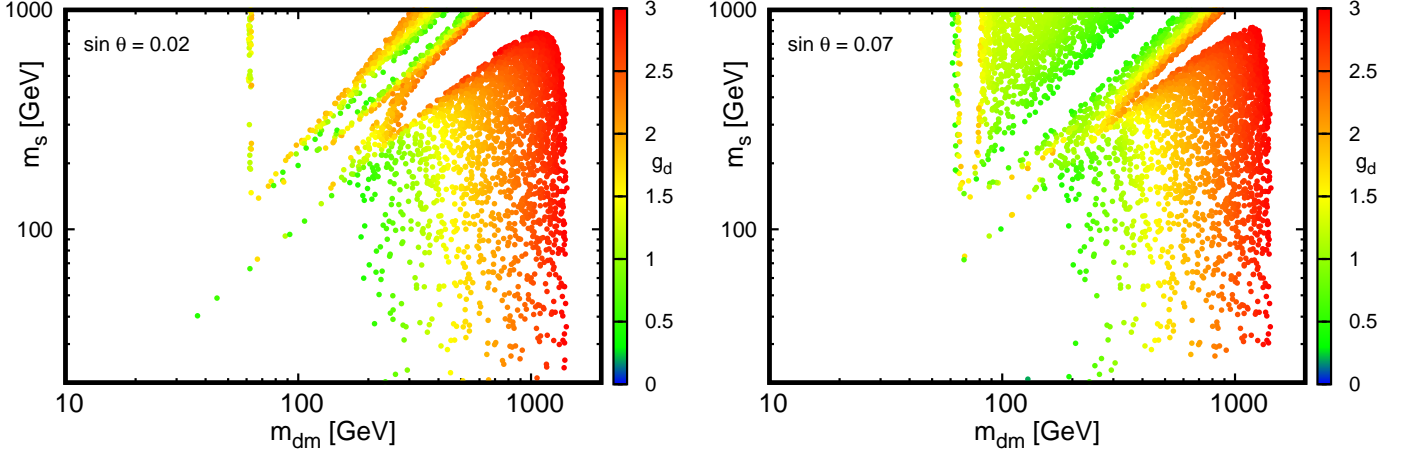


Figure 5: Viable regions in the parameter space residing above the neutrino floor and below the current direct detection exclusion bounds are shown. Constraints from the observed relic density and the invisible Higgs decay are applied as well. In the left plot, mixing angle is such that $\sin \theta = 0.02$ and in the right plot $\sin \theta = 0.07$. In both plots, $g_3 = 200$ GeV. The vertical color spectrum indicates the range of the dark coupling, g_d .

$g_d \lesssim 1$ there are still regions with $m_{\text{dm}} \lesssim 400$ GeV which are within reach in the future direct detection experiments.

Concerning indirect detection of DM, the Fermi Large Area Telescope (Fermi-LAT) collected gamma ray data from the Milky Way Dwarf Spheroidal Galaxies for six years [27]. The data indicates no significant gamma-ray excess. However, it can provide us with exclusion limits on the DM annihilation into $b\bar{b}$, $\tau\bar{\tau}$, $u\bar{u}$ and W^+W^- in the final state. As pointed out in [17] the Fermi-LAT data can exclude regions in the parameter space with $m_{\text{dm}} < 80$ GeV and also resonant region with $m_{\text{dm}} \sim m_s/2$.

A few comments are in order on the LHC constraints beside the invisible Higgs decay measurements. Concerning the mono-jet search in this scenario, it is pointed out in [17] that even in the region with $m_s > 2m_{\text{dm}}$ which has the largest production rate, the signal rate is more than one order of magnitude beneath the current LHC reach, having chosen the small mixing angle. In the same study it is found out that bounds corresponding to di-Higgs production at the LHC via the process $pp \rightarrow s \rightarrow hh$, with different final states ($4b, 2b2\gamma, 2b2\tau$) are not strong enough to exclude the pseudoscalar mass in the relevant range for small mixing angle as we chose in this study.

4 Conclusions

We revisited a DM model whose fermionic DM candidate has a pseudoscalar interaction with the SM quarks at tree level leading to the suppressed SI direct detection elastic cross section. In the present model we obtained analytically the leading loop diagrams contributing to the SI elastic scattering cross section.

Our numerical analysis taking into account the limits from the observed relic density, sug-

gests that regions with dark coupling $g_d \gtrsim 2.5$ and reasonable values for the other parameters, get excluded by DD upper bounds. It is also found that regions with $g_d \lesssim 0.25$ are excluded because they reside below the neutrino floor. However, a large portion of the parameter space stands above the neutrino floor remaining accessible in the future DD experiments such as XENONnT.

We also found regions of the parameter space above the neutrino floor while evading the current LUX/XENON1T DD upper limits, respecting the observed DM relic density and the invisible Higgs decay experimental bound. The viable region is slightly broadened for the moderate DM mass when $\sin \theta = 0.07$ in comparison with the case when $\sin \theta = 0.02$, both at $g_3 = 200$ GeV.

A Annihilation cross sections

The annihilation cross sections of a DM pair into a pair of the SM fermions are as the following

$$\begin{aligned} \sigma_{\text{ann}} v_{\text{rel}}(\bar{\psi}\psi \rightarrow \bar{f}f) &= \frac{g_d^2 \sin^2 2\theta}{64\pi} \left[\frac{1}{(s - m_h^2)^2 + m_h^2 \Gamma_h^2} + \frac{1}{(s - m_s^2)^2 + m_s^2 \Gamma_s^2} \right. \\ &\quad \left. - \frac{2(s - m_h^2)(s - m_s^2) + 2m_h m_s \Gamma_h \Gamma_s}{((s - m_h^2)^2 + m_h^2 \Gamma_h^2)((s - m_s^2)^2 + m_s^2 \Gamma_s^2)} \right] \times \\ &\quad \left(N_c \times 2s \left(\frac{m_f}{v_h} \right)^2 \left(1 - \frac{4m_f^2}{s} \right)^{\frac{3}{2}} \right), \end{aligned} \quad (12)$$

where the number of color charge is denoted by N_c . In the annihilation cross sections above the dominant contributions belong to the heavier final states $b\bar{b}$ and $t\bar{t}$. The total cross section into a pair of the gauge bosons (W^+W^- and ZZ) in the unitary gauge is given by

$$\begin{aligned} \sigma_{\text{ann}} v_{\text{rel}}(\bar{\psi}\psi \rightarrow W^+W^-, ZZ) &= \frac{g_d^2 \sin^2 2\theta}{64\pi} \left[\frac{1}{(s - m_h^2)^2 + m_h^2 \Gamma_h^2} + \frac{1}{(s - m_s^2)^2 + m_s^2 \Gamma_s^2} \right. \\ &\quad \left. - \frac{2(s - m_h^2)(s - m_s^2) + 2m_h m_s \Gamma_h \Gamma_s}{((s - m_h^2)^2 + m_h^2 \Gamma_h^2)((s - m_s^2)^2 + m_s^2 \Gamma_s^2)} \right] \times \\ &\quad \left[\left(\frac{m_W^2}{v_h} \right)^2 \left(2 + \frac{(s - 2m_W^2)^2}{4m_W^4} \right) \left(1 - \frac{4m_W^2}{s} \right)^{\frac{1}{2}} \right. \\ &\quad \left. + \frac{1}{2} \left(\frac{m_Z^2}{v_h} \right)^2 \left(2 + \frac{(s - 2m_Z^2)^2}{4m_Z^4} \right) \left(1 - \frac{4m_Z^2}{s} \right)^{\frac{1}{2}} \right]. \end{aligned} \quad (13)$$

And finally we obtain the following expression for the DM annihilation into two higgs bosons as

$$\begin{aligned}
\sigma_{\text{ann}} v_{\text{rel}}(\bar{\psi}\psi \rightarrow hh) &= \frac{g_d^2}{32\pi} \left(1 - \frac{4m_h^2}{s}\right)^{\frac{1}{2}} \left[\frac{a^2 \sin^2 \theta}{(s - m_h^2)^2 + m_h^2 \Gamma_h^2} + \frac{b^2 \cos^2 \theta}{(s - m_s^2)^2 + m_s^2 \Gamma_s^2} \right. \\
&\quad \left. + \frac{ab \sin 2\theta [(s - m_h^2)(s - m_s^2) + m_h m_s \Gamma_h \Gamma_s]}{((s - m_h^2)^2 + m_h^2 \Gamma_h^2)((s - m_s^2)^2 + m_s^2 \Gamma_s^2)} \right] \\
&\quad + \frac{g_d^4 \sin^4 \theta}{16\pi s} \left(1 - \frac{4m_h^2}{s}\right)^{\frac{1}{2}} \left[s(m_{\text{dm}}^2 - t) + m_{\text{dm}}^2 m_h^2 \right. \\
&\quad \left. - (m_{\text{dm}}^2 + m_h^2 - t)^2 \right] \times \left(\frac{1}{t - m_{\text{dm}}^2} + \frac{1}{u - m_{\text{dm}}^2} \right)^2,
\end{aligned} \tag{14}$$

with

$$\begin{aligned}
a &= 3 \cos^2 \theta \sin \theta g_1 + 6 \sin^2 \theta \cos \theta g_2 v_h + 6 \cos^3 \theta \lambda v_h + \sin^3 \theta g_3, \\
b &= 3 \cos \theta \sin^2 \theta g_1 - \cos \theta g_1 + 6 \sin^3 \theta g_2 v_h - 4 \sin \theta g_2 v_h + 6 \cos^2 \theta \sin \theta \lambda v_h,
\end{aligned} \tag{15}$$

and DM annihilation into two s bosons as

$$\begin{aligned}
\sigma_{\text{ann}} v_{\text{rel}}(\bar{\psi}\psi \rightarrow ss) &= \frac{g_d^2}{32\pi} \left(1 - \frac{4m_s^2}{s}\right)^{\frac{1}{2}} \left[\frac{c^2 \sin^2 \theta}{(s - m_h^2)^2 + m_h^2 \Gamma_h^2} + \frac{d^2 \cos^2 \theta}{(s - m_s^2)^2 + m_s^2 \Gamma_s^2} \right. \\
&\quad \left. + \frac{c d \sin 2\theta [(s - m_h^2)(s - m_s^2) + m_h m_s \Gamma_h \Gamma_s]}{((s - m_h^2)^2 + m_h^2 \Gamma_h^2)((s - m_s^2)^2 + m_s^2 \Gamma_s^2)} \right] \\
&\quad + \frac{g_d^4 \cos^4 \theta}{16\pi s} \left(1 - \frac{4m_s^2}{s}\right)^{\frac{1}{2}} \left[s(m_{\text{dm}}^2 - t) + m_{\text{dm}}^2 m_s^2 \right. \\
&\quad \left. - (m_{\text{dm}}^2 + m_s^2 - t)^2 \right] \times \left(\frac{1}{t - m_{\text{dm}}^2} + \frac{1}{u - m_{\text{dm}}^2} \right)^2,
\end{aligned} \tag{16}$$

with

$$\begin{aligned}
c &= 3 \sin^3 \theta g_1 - 2 \sin \theta g_1 - 6 \cos \theta \sin^2 \theta g_2 v_h + 2 \cos \theta g_2 v_h \\
&\quad + 6 \cos \theta \sin^2 \theta \lambda v_h + \cos^2 \theta \sin \theta g_3, \\
d &= 3 \cos \theta \sin^2 \theta g_1 - 6 \cos^2 \theta \sin \theta g_2 v_h - 6 \sin^3 \theta \lambda v_h + \cos^3 \theta g_3.
\end{aligned} \tag{17}$$

The Mandelstam variables are denoted by s , t and u .

B DD cross section at tree level and loop-level

At *tree level* the DD cross section is

$$\sigma_{\text{SI}}^p \sim \frac{0.28^2 m_p^6 m_{\text{dm}}^2 g_d^2}{2\pi v_h^2 (m_p + m_{\text{dm}})^4} \left(\frac{1}{m_h^2} - \frac{1}{m_s^2} \right)^2 v_{\text{dm}}^2, \tag{18}$$

and the DD cross section at *loop level* reads

$$\begin{aligned}
\sigma_{\text{SI}}^p &\sim \frac{0.28^2 m_p^4 m_{\text{dm}}^4 g_d^4}{64\pi^5 v_h^2 (m_p + m_{\text{dm}})^2} \left| \frac{\cos \theta}{m_h^2} C_{hhh} F(\beta_h) + \frac{\cos \theta}{m_h^2} C_{hsh} F(\beta_h, \beta_s) + \frac{\cos \theta}{m_h^2} C_{ssh} F(\beta_s) \right. \\
&\quad \left. - \frac{\sin \theta}{m_s^2} C_{hhs} F(\beta_h) - \frac{\sin \theta}{m_s^2} C_{hss} F(\beta_h, \beta_s) - \frac{\sin \theta}{m_s^2} C_{sss} F(\beta_s) \right|^2,
\end{aligned} \tag{19}$$

where, m_p is the proton mass, $v_h = 246$ GeV, $\beta_h = m_h^2/m_{\text{dm}}^2$ and $\beta_s = m_s^2/m_{\text{dm}}^2$.

We present the relevant loop function in the case $\beta_i \neq \beta_j$, as

$$m_{\text{dm}}^2 F(\beta_i, \beta_j) = -\frac{1}{2} + \frac{\sqrt{\beta_j - 4}}{4(\beta_j - \beta_i)} \beta_j^{3/2} \log \frac{\sqrt{\beta_j^2 - 4\beta_j} + \beta_j - 2}{\sqrt{\beta_j^2 - 4\beta_j} - \beta_j - 2} \\ - \frac{\sqrt{\beta_j - 4}}{4(\beta_j - \beta_i)} \beta_j^{3/2} \log \frac{\sqrt{\beta_j - 4} + \sqrt{\beta_j}}{\sqrt{\beta_j - 4} - \sqrt{\beta_j}} - (\beta_j^2 - 2\beta_j) \log \beta_j - (\beta_j \rightarrow \beta_i), \quad (20)$$

and when $\beta_i = \beta_j = \beta$, the loop function F reads,

$$m_{\text{dm}}^2 F(\beta) = -\frac{1}{4} + \frac{1}{4(\beta - 4)} \left[2(\beta - 3) \sqrt{\beta^2 - 4\beta} \log \frac{\sqrt{\beta - 4} + \sqrt{\beta}}{\sqrt{\beta - 4} - \sqrt{\beta}} \right. \\ \left. + 2(\beta^2 - 5\beta + 4) \log \beta + 2(\beta - 3) \log \frac{\beta^2 - 4\beta - (\beta - 2) \sqrt{\beta^2 - 4\beta}}{\beta^2 - 4\beta + (\beta - 2) \sqrt{\beta^2 - 4\beta}} \right]. \quad (21)$$

The trilinear scalar couplings are

$$C_{hhh} = -6g_2 v_h \sin^2 \theta \cos \theta - 3g_1 \cos^2 \theta \sin \theta - 6\lambda v_h \cos^3 \theta - g_3 \sin^3 \theta, \\ C_{hhs} = g_2 v_h (6 \sin^3 \theta - 4 \sin \theta) + 3g_1 \sin^2 \theta \cos \theta - g_1 \cos \theta \\ + 6\lambda v_h \cos^2 \theta \sin \theta - g_3 \sin^2 \theta \cos \theta, \\ C_{ssh} = g_2 v_h (6 \sin^2 \theta \cos \theta - 2 \cos \theta) + (2 \sin \theta - 3 \sin^3 \theta) g_1 \\ - 6\lambda v_h \sin^2 \theta \cos \theta - g_3 \cos^2 \theta \sin \theta, \\ C_{sss} = 6g_2 v_h \cos^2 \theta \sin \theta - 3g_1 \sin^2 \theta \cos \theta + 6\lambda v_h \sin^3 \theta - g_3 \cos^3 \theta. \quad (22)$$

References

- [1] **Planck** Collaboration, P. A. R. Ade *et al.*, “Planck 2013 results. XVI. Cosmological parameters,” *Astron. Astrophys.* **571** (2014) A16, [arXiv:1303.5076 \[astro-ph.CO\]](#).
- [2] **WMAP** Collaboration, G. Hinshaw *et al.*, “Nine-year wilkinson microwave anisotropy probe (wmap) observations: Cosmological parameter results,” *Astrophys.J.Suppl.* **208** (2013) 19, [arXiv:1212.5226 \[astro-ph\]](#).
- [3] **LUX** Collaboration, D. S. Akerib *et al.*, “Results from a search for dark matter in the complete LUX exposure,” *Phys. Rev. Lett.* **118** no. 2, (2017) 021303, [arXiv:1608.07648 \[astro-ph.CO\]](#).
- [4] **XENON** Collaboration, E. Aprile *et al.*, “First Dark Matter Search Results from the XENON1T Experiment,” *Phys. Rev. Lett.* **119** no. 18, (2017) 181301, [arXiv:1705.06655 \[astro-ph.CO\]](#).
- [5] **PandaX-II** Collaboration, X. Cui *et al.*, “Dark Matter Results From 54-Ton-Day Exposure of PandaX-II Experiment,” *Phys. Rev. Lett.* **119** no. 18, (2017) 181302, [arXiv:1708.06917 \[astro-ph.CO\]](#).

- [6] A. L. Fitzpatrick, W. Haxton, E. Katz, N. Lubbers, and Y. Xu, “The Effective Field Theory of Dark Matter Direct Detection,” *JCAP* **1302** (2013) 004, [arXiv:1203.3542 \[hep-ph\]](#).
- [7] G. Arcadi, M. Lindner, F. S. Queiroz, W. Rodejohann, and S. Vogl, “Pseudoscalar Mediators: A WIMP model at the Neutrino Floor,” *JCAP* **1803** no. 03, (2018) 042, [arXiv:1711.02110 \[hep-ph\]](#).
- [8] N. F. Bell, G. Busoni, and I. W. Sanderson, “Loop Effects in Direct Detection,” *JCAP* **1808** no. 08, (2018) 017, [arXiv:1803.01574 \[hep-ph\]](#).
- [9] T. Abe, M. Fujiwara, and J. Hisano, “Loop corrections to dark matter direct detection in a pseudoscalar mediator dark matter model,” [arXiv:1810.01039 \[hep-ph\]](#).
- [10] T. Li, “Revisiting the direct detection of dark matter in simplified models,” *Phys. Lett. B* **782** (2018) 497–502, [arXiv:1804.02120 \[hep-ph\]](#).
- [11] J. Herrero-Garcia, E. Molinaro, and M. A. Schmidt, “Dark matter direct detection of a fermionic singlet at one loop,” *Eur. Phys. J. C* **78** no. 6, (2018) 471, [arXiv:1803.05660 \[hep-ph\]](#).
- [12] J. Hisano, R. Nagai, and N. Nagata, “Singlet Dirac Fermion Dark Matter with Mediators at Loop,” [arXiv:1808.06301 \[hep-ph\]](#).
- [13] T. Han, H. Liu, S. Mukhopadhyay, and X. Wang, “Dark Matter Blind Spots at One-Loop,” [arXiv:1810.04679 \[hep-ph\]](#).
- [14] D. Azevedo, M. Duch, B. Grzadkowski, D. Huang, M. Iglicki, and R. Santos, “One-loop contribution to dark matter-nucleon scattering in the pseudoscalar dark matter model,” [arXiv:1810.06105 \[hep-ph\]](#).
- [15] K. Ishiwata and T. Toma, “Probing pseudo scalar dark matter at loop level,” [arXiv:1810.08139 \[hep-ph\]](#).
- [16] K. Ghorbani, “Fermionic dark matter with pseudo-scalar Yukawa interaction,” *JCAP* **1501** (2015) 015, [arXiv:1408.4929 \[hep-ph\]](#).
- [17] S. Baek, P. Ko, and J. Li, “Minimal renormalizable simplified dark matter model with a pseudoscalar mediator,” [arXiv:1701.04131 \[hep-ph\]](#).
- [18] P. H. Ghorbani, “Electroweak Baryogenesis and Dark Matter via a Pseudoscalar vs. Scalar,” [arXiv:1703.06506 \[hep-ph\]](#).
- [19] CMS Collaboration, V. Khachatryan *et al.*, “Searches for invisible decays of the Higgs boson in pp collisions at $\sqrt{s} = 7, 8$, and 13 TeV,” *JHEP* **02** (2017) 135, [arXiv:1610.09218 \[hep-ex\]](#).
- [20] K. Ghorbani and L. Khalkhali, “Mono-higgs signature in a fermionic dark matter model,” *Journal of Physics G: Nuclear and Particle Physics* **44** no. 10, (2017) 105004.

- [21] D. Barducci, G. Belanger, J. Bernon, F. Boudjema, J. Da Silva, S. Kraml, U. Laa, and A. Pukhov, “Collider limits on new physics within micrOMEGAs4.3” *Comput. Phys. Commun.* **222** (2018) 327–338, [arXiv:1606.03834 \[hep-ph\]](#).
- [22] **Planck** Collaboration, P. A. R. Ade *et al.*, “Planck 2015 results. XIII. Cosmological parameters,” *Astron. Astrophys.* **594** (2016) A13, [arXiv:1502.01589 \[astro-ph.CO\]](#).
- [23] B. W. Lee and S. Weinberg, “Cosmological Lower Bound on Heavy Neutrino Masses,” *Phys. Rev. Lett.* **39** (1977) 165–168.
- [24] J. Billard, L. Strigari, and E. Figueroa-Feliciano, “Implication of neutrino backgrounds on the reach of next generation dark matter direct detection experiments,” *Phys. Rev.* **D89** no. 2, (2014) 023524, [arXiv:1307.5458 \[hep-ph\]](#).
- [25] S. Ipek, D. McKeen, and A. E. Nelson, “A Renormalizable Model for the Galactic Center Gamma Ray Excess from Dark Matter Annihilation,” *Phys. Rev.* **D90** no. 5, (2014) 055021, [arXiv:1404.3716 \[hep-ph\]](#).
- [26] G. Belanger, F. Boudjema, A. Pukhov, and A. Semenov, “micrOMEGAs 3: A program for calculating dark matter observables,” *Comput. Phys. Commun.* **185** (2014) 960–985, [arXiv:1305.0237 \[hep-ph\]](#).
- [27] **Fermi-LAT** Collaboration, M. Ackermann *et al.*, “Searching for Dark Matter Annihilation from Milky Way Dwarf Spheroidal Galaxies with Six Years of Fermi Large Area Telescope Data,” *Phys. Rev. Lett.* **115** no. 23, (2015) 231301, [arXiv:1503.02641 \[astro-ph.HE\]](#).